J. Biochem. **133**, 467–474 (2003)
DOI: 10.1093/jb/mvg061

Crystal Structures of β-Amylase from *Bacillus cereus* var. *mycoides* in Complexes with Substrate Analogs and Affinity-Labeling Reagents

Takuji Oyama*[,1], Hideo Miyake[1], Masami Kusunoki[2] and Yasunori Nitta†[,1]

[1]Laboratory of Enzyme Chemistry, Graduate School of Agriculture and Biological Science, Osaka Prefecture University, Sakai, Osaka 599-8531, and [2]Institute for Protein Research, Osaka University, Suita, Osaka 565-0871

Received November 26, 2002; accepted January 24, 2003

The crystal structures of β-amylase from *Bacillus cereus* var. *mycoides* in complexes with five inhibitors were solved. The inhibitors used were three substrate analogs, *i.e.* glucose, maltose (product), and a synthesized compound, *O*-α-D-glucopyranosyl-(1→4)-*O*-α-D-glucopyranosyl-(1→4)-D-xylopyranose (GGX), and two affinity-labeling reagents with an epoxy alkyl group at the reducing end of glucose. For all inhibitors, one molecule was bound at the active site cleft and the non-reducing end glucose of the four inhibitors except GGX was located at subsite 1, accompanied by a large conformational change of the flexible loop (residues 93–97), which covered the bound inhibitor. In addition, another molecule of maltose or GGX was bound about 30 Å away from the active site. A large movement of residues 330 and 331 around subsite 3 was also observed upon the binding of GGX at subsites 3 to 5. Two affinity-labeling reagents, α-EPG and α-EBG, were covalently bound to a catalytic residue (Glu-172). A substrate recognition mechanism for the β-amylase was discussed based on the modes of binding of these inhibitors in the active site cleft.

Key words: active site cleft, affinity-labeling reagent, *Bacillus cereus*, β-amylase, crystal structure, subsite structure.

Abbreviations: α-EPG, 2,3-epoxypropyl α-D-glucopyranoside; α-EBG, 3,4-epoxybutyl α-D-glucopyranoside; BCM, *Bacillus cereus* var. *mycoides*; GGX, *O*-α-D-glucopyranosyl-(1→4)-*O*-α-D-glucopyranosyl-(1→4)-D-xylopyranose.

β-Amylase [EC 3.2.1.2] is an exo-enzyme that catalyzes the hydrolysis of the α-1,4-glucosidic linkage of a substrate such as starch and liberates β-maltose from the non-reducing end. It is a member of family 14 of the sequence-based classification of glycoside hydrolases (*1*). β-Amylases are only distributed in higher plants and certain bacteria, and there are some differences between bacterial and plant β-amylases. β-Amylases from bacteria have the ability to bind and hydrolyze raw starch whereas plant β-amylases do not. This binding ability is attributable to a starch-binding domain located at the C-terminus of the sequence (*2*). Bacterial β-amylases exhibit maximum catalytic activity at neutral pH while plant enzymes do so under weak acidic conditions. Furthermore, the intrinsic breakdown rate constant of the α-1,4-glucosidic linkage (k_{int}) for β-amylase from *Bacillus cereus* var. *mycoides* (abbreviated as BCM β-amylase) was more than five times as high as those of plant β-amylases, indicating a subtle structural difference in the active site between β-amylases from the two origins (*3*).

Recently, the crystal structures of several bacterial and plant β-amylases have been determined (*4–7*). All β-amylases possess $(\beta/\alpha)_8$ barrels in their catalytic domains, where the active site clefts are located on the carboxyl side of the central β-strands. The C-terminal starch-binding domains of bacterial β-amylases exhibit similar folds to those of cyclodextrin glucosyltransferase (CGTase) (*8*, *9*) and glucoamylase (*10*). Both bacterial and plant β-amylases bind maltose molecules to the active sites with similar binding modes, suggesting the basic conservation of the catalytic mechanism (*4–7*). Mikami *et al.* have suggested that the difference in optimum pH of the catalytic activity between bacterial and plant β-amylases could be due to the different locations of the amino acid residues around the catalytic residues (*4*).

Nitta *et al.* have designed and synthesized several inhibitors for β-amylase, and kinetically characterized them to elucidate the catalytic mechanism (*11–13*). 2,3-Epoxypropyl-α-D-glucopyranoside (α-EPG) (Fig. 1d) is an affinity-labeling reagent that irreversibly inactivates β-amylase by making a covalent bond with a catalytic residue (*11*). Glu-186 of soybean β-amylase has been identified as a catalytic residue affinity-labeled by α-EPG (*12*). *O*-α-D-glucopyranosyl-(1→4)-*O*-α-D-glucopyranosyl-(1→4)-D-xylopyranose (GGX) (Fig. 1c) is a compound in which the reducing end glucose of maltotriose is replaced by xylose (*13*). This compound is a specific competitive inhibitor of soybean β-amylase and has almost the same binding affinity as maltotriose, a substrate, and the xylose residue in GGX has a stable C_1 pyranose-ring structure. Therefore, it was presumed that GGX is bound at subsites 1 to 3 in a pseudo-productive manner. If so, it is expected that the second glucose residue and the xylose one straddle the two catalytic residues located between subsites 2 and 3, preventing the hydrolysis

*Present address: Department of Structural Biology, Biomolecular Engineering Research Institute, 6-2-3 Furuedai, Suita, Osaka 565-0874.
†To whom correspondence should be addressed. Tel: +81-72-254-9473, Fax: +81-072-254-9474, E-mail: nitta@biochem.osakafu-u.ac.jp

Fig. 1. **Chemical structures of the substrate analogs and the affinity-labeling reagents.**

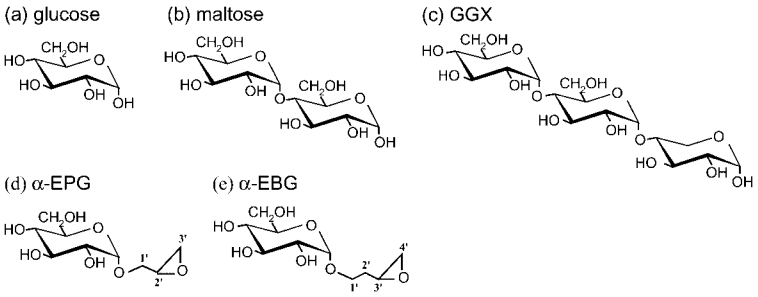

between the second glucose and the xylose. The crystal structures of β-amylase in complexes with such covalently or strongly bound inhibitors are expected to reveal the precise interactions between the enzyme and the inhibitors, and thus they should be useful for understanding the catalytic mechanism of β-amylase. In our previous study, we determined the three-dimensional structure of BCM β-amylase, which consists of a single polypeptide chain of 516 amino acids and possesses six subsites in the active site cleft (*3*). In the present study, we examine X-ray crystal structures of BCM β-amylase in complexes with α-EPG, α-EBG, GGX, glucose and maltose (Fig. 1), and analyze the substrate recognition mechanism of this enzyme based on the structural data obtained.

EXPERIMENTAL PROCEDURES

Native crystals of BCM β-amylase were prepared as described previously (*5*). The crystals belong to space group *C*2, with unit cell constants of a = 177.9 Å, b = 112.9 Å, c = 146.2 Å, and β = 105.8°, with four enzyme

Table 1. **Data collection and refinement statistics for the β-amylase/inhibitor complexes.**

		Data collection statistics				
Inhibitors		Glucose	maltose	GGX	α-EPG	α-EBG
Soaking concentration	(mM)	200	100	50	50	50
Soaking time (d)		2	2	7	2	2
No. of crystals		1	1	2	4	1
Overall resolution range	(Å)	39.5–2.00	65.6–2.00	42.6–2.00	95.4–1.90	73.4–2.00
Outermost resolution bin	(Å)	2.09–2.00	2.09–2.00	2.09–2.00	1.99–1.90	2.09–2.00
No. of observed reflections		243,229	223,201	322,908	365,923	257,638
No. of unique reflections	overall	135,775	119,820	154,446	143,718	128,094
	outermost	12,350	6,542	14,111	10,261	6,376
Completeness (%)	overall	72.8	64.5	82.3	66.4	68.6
	outermost	53.1	28.3	60.4	38.1	27.4
I/sig(I)	overall	17.9	9.9	19.2	17.6	9.5
	outermost	3.1	1.8	2.7	2.8	1.8
Redundancy	overall	1.8	1.9	2.1	2.6	2.0
	outermost	1.5	1.3	1.6	1.5	1.2
R_{merge}[a]	overall	0.062	0.073	0.060	0.064	0.087
	outermost	0.214	0.226	0.217	0.288	0.247
		Refinement statistics				
No. of protein atoms		16,476	16,476	16,476	16,476	16,476
No. of saccharide atoms		48	184	248	64	68
No. of solvent molecules		639	310	482	432	379
Resolution range	(Å)	8.0–2.1	8.0–2.2	8.0–2.1	8.0–2.0	8.0–2.1
No. of independent reflections		120,273	100,909	136,111	129,785	117,890
Completeness	(%)	75.7	73.2	85.7	70.4	74.2
R-factor[b]/free-R[c]		0.179/0.236	0.186/0.238	0.189/0.239	0.200/0.246	0.198/0.253
Average B-factor (Å^2) for protein atoms		23.9	20.2	27.5	17.1	21.5
saccharide atoms		25.5	27.0	46.8	16.7	20.0
r.m.s. deviations from ideality for protein						
bond length	(Å)	0.007	0.006	0.007	0.007	0.007
bond angle	(°)	1.476	1.396	1.451	1.708	1.478
for saccharide						
bond length	(Å)	0.007	0.007	0.006	0.016	0.011
bond angle	(°)	1.233	1.063	1.181	2.169	1.903

[a]$R_{merge} = \Sigma_{hkl}\Sigma_i |I(hkl)_i - \langle I(hkl)\rangle| / \Sigma_{hkl}\Sigma_i I(hkl)_i$, where $I(hkl)_i$ is the ith measurement of reflection hkl, $\langle I(hkl)\rangle$ the mean value of equivalent reflections, and i runs through the symmetry-related reflections. [b]R-factor=$\Sigma||F_{obs}| - |F_{calc}||/\Sigma|F_{obs}|$, where $|F_{obs}|$ and $|F_{calc}|$ are the observed and calculated structure factor amplitudes, respectively. [c]R_{free} factor was calculated using 5% of the data.

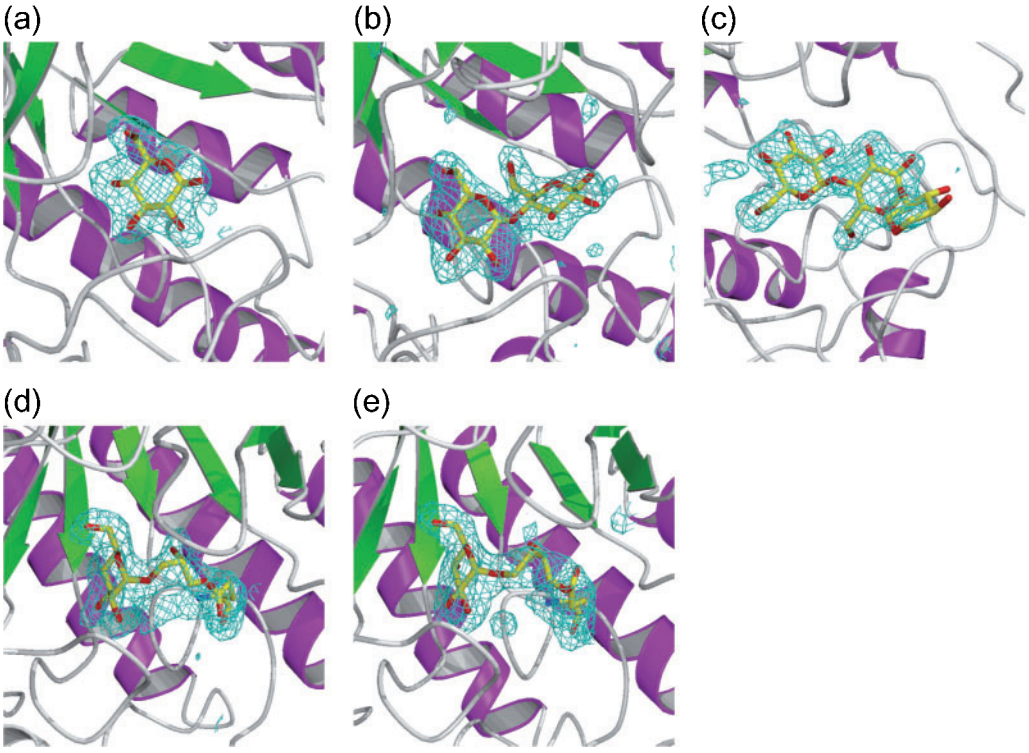

Fig. 2. **Gallery of omit $|F_o - F_c|$ electron density maps countered at 3 σ(ρ).** (a) Glucose; (b) maltose; (c) GGX; (d) α-EPG; (e) α-EBG. Figures were prepared with BOBSCRIPT (*24*).

molecules per asymmetric unit. Crystals of the enzyme in a complex with each inhibitor were prepared by soaking native crystals in artificial mother liquor comprising 50 mM Na-phosphate (pH 7.0), 15% (w/v) PEG6000, and each inhibitor. Glucose and maltose were purchased from Hayashibara Seikagaku Kogyo. GGX and α-EPG were synthesized as described (*13*, *11*). 3,4-Epoxybutyl α-D-glucopyranoside (α-EBG) was synthesized by the same method as that for α-EPG. X-ray diffraction data for crystals of the α-EPG complex were collected at 293 K with synchrotron radiation (SR) at the beamline BL-18B, operated at 2.5 GeV, of the Photon Factory (PF) at the High Energy Accelerator Research Organization, Tsukuba, Japan. The X-ray beam was monochromatized to 1.0000 Å with a Si(111) monochromator and was collimated with a 0.2 mm square aperture. Oscillation photographs were recorded on 200 mm × 400 mm imaging plates mounted on a screenless Weissenberg camera for macromolecular crystals (*14*) with a cylindrical cassette of 430 mm radius. X-ray data for the other enzyme/inhibitor crystals were collected at 293 K with a RIGAKU R-AXIS IIc or R-AXIS IV imaging plate diffractometer mounted on a RIGAKU RU-200 rotating-anode generator operated at 40 kV and 100 mA. The Cu*K*α radiation was monochromatized with either a graphite-monochromator (R-AXIS IIc) or a double-mirror optical system (R-AXIS IV). All the diffraction data sets were processed with program DENZO/SCALEPACK (*15*). The statistics for intensity data sets are given in Table 1.

The crystal structure of free BCM β-amylase at pH 7.0 is essentially the same as that at pH 9.0 reported previously (*5*), and the structure at pH 7.0 was used as a starting model for structure refinement of the enzyme/inhibitor complexes. The inhibitors bound to the enzyme could be clearly identified in ($|F_{obs}| - |F_{calc}|$) difference Fourier electron density maps (Fig. 2). Inhibitor models were built manually with program O (*16*). The structures were then refined with program X-PLOR (*17*), the prepstage, slowcool and B-factor refinement stages being carried out in that order with Engh and Huber parameters (*18*). The crystallographic refinement and subsequent manual corrections of the models were iterated until convergence of the refinement (Table 1). Radiation damage to the crystals during data collection at room temperature led to low completeness and redundancy of each diffraction data set. Therefore, to avoid the model bias from the starting model and the misinterpretation of electron density maps, the model refinement was carefully iterated using a lot of omit electron density maps for each refinement cycle. Analyses of the enzyme/inhibitor complexes with program PROCHECK (*19*) showed that all amino acid residues except for glycine or proline are in allowed regions of a Ramachandron plot (data not shown).

RESULTS AND DISCUSSION

Structures of BCM β-Amylase in Complexes with Inhibitors—The main chain folds for the five BCM β-amylase/inhibitor complexes are almost identical to that of the free enzyme, which has three domains: an N-terminal catalytic domain (domain A) with a $(\beta/\alpha)_8$ barrel at the center of the molecule, domain B consisting of three long loops extending from domain A, and a C-terminal domain (domain C) with two β-sheets of almost anti-parallel pairs of β-strands (Fig. 3a) (*5*). Two conserved catalytic residues, Glu172 and Glu367, are located near subsites 2 and 3 in the active site (*5*). For each complex, one molecule of inhibitor was bound to the active site cleft located

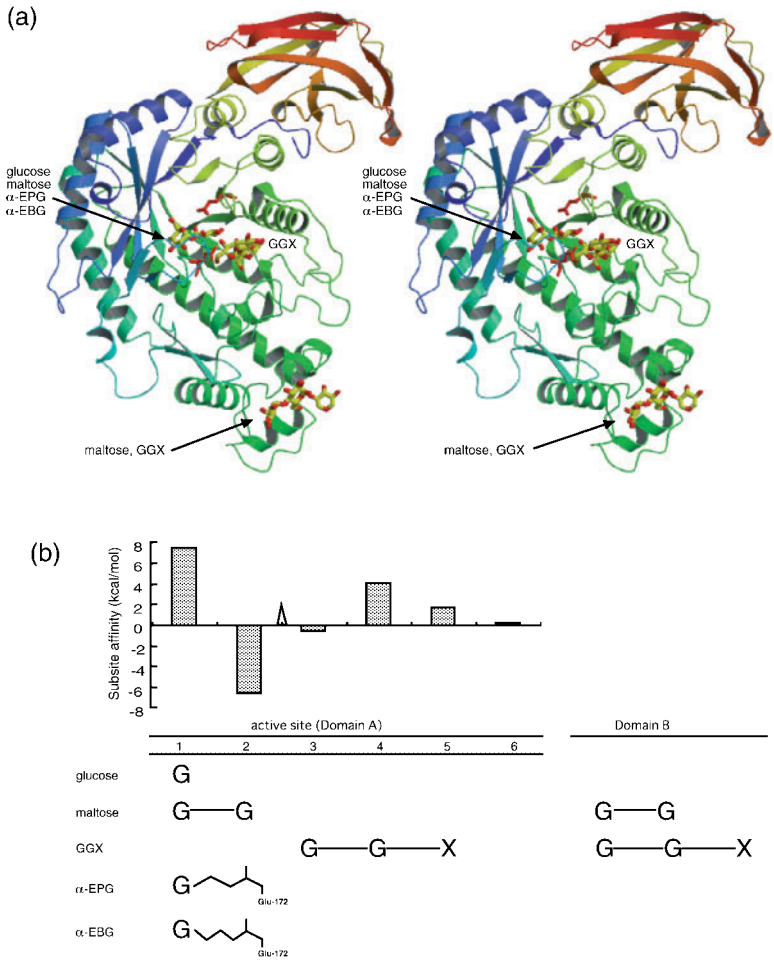

Fig. 3. **(a) Ribbon representation of BCM β-amylase obtained with programs MOLSCRIPT (*25*) and RATER 3D (*26*).** The enzyme molecule is coloured in a rainbow gradation from blue (N-terminus) to red (C-terminus). Saccharide binding sites are indicated by arrows. Only maltose and GGX are presented as stick models for clarity. **(b) Summary of saccharide binding in the active site and at domain B.** The subsite numbers run from the non-reducing end of the substrate starting with unity. The subsite affinities estimated by kinetic analysis are quoted from Nitta *et al.* (*3*). Subsite 1 is located at the bottom of the active site cleft and binds a glucose residue at the non-reducing end of oligosaccharides. The cleavage position on the substrate between subsites 2 and 3 is indicated by an arrowhead.

at the carboxyl side of the central β-sheet of domain A. Two affinity-labeling reagents, α-EPG and α-EBG, are covalently bound to a catalytic residue Glu-172. Two modes of local conformational changes were observed upon the binding of inhibitors to the active site. The first one was a large movement of the peptide segment of residues 93–97 (the flexible loop) to the active site cleft, which was observed in the respective complexes with glucose, maltose, α-EPG and α-EBG (Figs. 4 and 5). In these complexes, the non-reducing glucose residue of the inhibitor was bound to subsite 1 at the bottom of the cleft. The flexible loop moved to form a part of the substrate-binding site by changing its conformation from an open form in the free enzyme to a closed form. Such movements have also been seen for both bacterial and plant β-amylases complexed with maltose (*4*, *6*, *7*). The second mode of local conformation change was observed in the BCM β-amylase/GGX complex, where two amino acid residues, Thr-330 and Cys-331, around subsite 3 shifted greatly from the free enzyme to interact with the non-reducing end glucose of GGX bound at subsites 3 to 5 (Fig. 5). A second binding site for maltose and GGX was found in domain B outside of the catalytic cleft about 30 Å apart from the catalytic residues (Fig. 3a). This binding site, which is supposed to be involved in the binding of this enzyme to raw-starch (*4*), seems to need a maltose unit to interact with a saccharide, because glucose, α-EPG, and α-EBG containing a single glucose residue were not bound to this site. Domain C also has a maltose binding site, in which the hydrophobic side chains of Trp-449 and Trp-495 predominantly contribute to the interaction with a saccharide (*4*). In the present study, however, no inhibitors bound there. It is thought that this was because of the steric hindrance due to the crystal packing of the enzyme (*5*).

Saccharide Binding at Subsite 1—In the subsite structure of BCM β-amylase evaluated according to Hiromi's theory, subsites 1 and 4 exhibit great positive subsite-affinity to glucose residues, whereas subsites 2 and 3 spanning a pair of catalytic residues exhibit negative affinity (*3*) (Fig. 3b). In the complex with glucose, the enzyme binds only one glucose molecule at subsite 1 with the highest affinity (Fig. 4a), and the flexible loop adopts a closed conformation, almost completely shielding the bound glucose from the solvent. This loop is highly ordered in the crystal as compared to that in the free β-amylase. The glucose molecule undergoes many interactions with the enzyme: a total of eight hydrogen bonds directly with Asp-49, His-89, and Arg-397, and Asp-97, and through a water molecule with Asn-94 and Lys-287. The averaged temperature factor (*B*-factor) was low (19.8 Å). Asn-94 and Asp-97 are part of the flexible loop in the closed form. These extensive interactions would account for the highest affinity of subsite 1 among the six subsites.

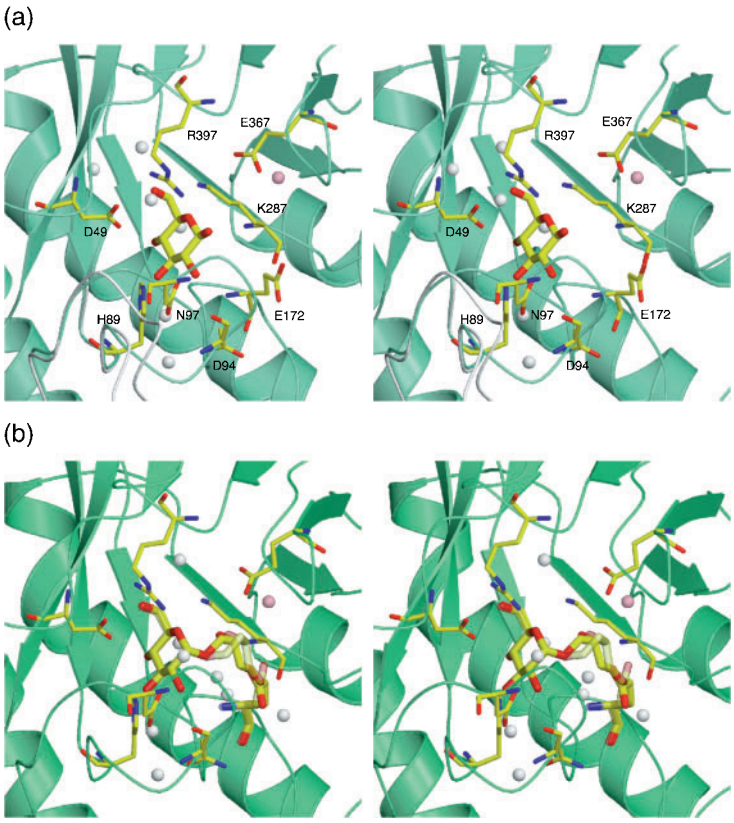

Fig. 4. **Close-up views of binding of (a) glucose and (b) an affinity-labeling reagent at subsite 1.** Amino acid residues interacting with the inhibitors through hydrogen bonds are presented as stick models. The two catalytic residues (Glu-172 and Glu-367) are also depicted. Oxygen, nitrogen, and carbon atoms are colored red, blue, and yellow, respectively. Water molecules are denoted by white spheres. The nucleophilic attacking water bound to the Glu-367 sidechain is depicted as pink a sphere. The flexible loop (residues93–97) with an open form in the free-enzyme (*5*) in presented as a while tube. α-EBG is represented by a transparent model in (b).

A glucose residue in both α-EPG and α-EBG was bound at subsite 1 and the epoxide formed a covalent bond to the carboxyl group of Glu-172 (Fig. 4b). This binding mode is consistent with that proposed for the affinity-labeling of soybean β-amylase by α-EPG (*12*). α-EPG and α-EBG were prepared as a racemic mixture as to the 2′- and 3′-carbon atoms, respectively. Structure analyses indicated that the *R*-stereoisomers of these inhibitors were selectively bound to the enzyme during soaking of the crystals. The B-factor of the flexible loop was remarkably lower than those in the complexes with the other inhibitors: the B-factor value of the flexible loop in the complexes with the affinity-labeling reagent was similar to that of the rest of the polypeptidechain, whereas that in the other complexes was more than twice as high as that of the rest (Table 1). This implies that the flexible loop of the affinity-labeled enzyme has a completely closed and fixed conformation.

Binding of Maltose and GGX in the Active Site Cleft of the β-Amylase—In the active site cleft of the BCM β-amylase/maltose complex, only one β-maltose molecule was observed, which was bound at subsites 1 and 2 (Fig. 5a). As for the β-amylases from soybean and *Bacillus cereus* BQ10-S1 SpoII, another maltose is bound at subsites 3 and 4, and for barley β-amylase, one glucose residue is observed at subsite 4 in addition to subsites 1 and 2 (*4*, *6*, *7*). No saccharide residue, however, was observed at subsites 3 and 4 in the present enzyme/maltose complex. The reducing end glucose (Glc2) of maltose interacts with β-amylase at subsite 2 through mainly hydrogen bonds, as in the case of Glc1: hydrogen bonds were observed with the main chain atoms of Val-95 and Ala-369, and the side chain atoms of Glu-172, Lys-287, Thr-330, and Glu-367.

In contrast to the four inhibitors described above, GGX is bound to the active site cleft of the β-amylase at subsites 3 to 5 (Fig. 5b). The glucose residue (Glc3) of GGX at subsite 3 is bound to the enzyme through several hydrogen bonds. Thr-330 and Cys-331 around subsite 3 shifts about 1.7 Å and 1.5 Å toward the active site, respectively, upon complex formation. As a result, the side chain of Thr-330 is involved in the polar interaction of the enzyme with GGX. Although the β-amylase/maltooligosaccharide interactions at subsite 1 to 3 are mainly polar ones, glucose and xylose residues at subsites 4 and 5 (Glc4 and Xyl5) in GGX interact with the enzyme mainly through hydrophobic interactions, in particular with Tyr-186 and Leu-370. The side chain of His-292 forms the sole hydrogen bond with glucose at subsite 4, while no hydrogen bond is observed for the binding of the xylose residue at subsite 5 (Fig. 4).

As shown in Fig. 6, we propose a productive binding model for maltopentaose (G5) in the active site cleft based on the binding data for maltose at subsites 1 and 2, and GGX at subsites 3 to 5. It was built as follows: Firstly, the Cα atoms of the β-amylase/maltose complex were least-squares fitted to those of the enzyme/GGX complex (with a root mean square distance of 0.78 Å). In the superimposed structure, the O4 atom of Glc3 in GGX was 1.5 Å apart from the C1 atom of Glc2 in maltose. An initial G5 model was built from the maltose and the GGX by forcibly forming an α-1,4-glucosidic linkage between Glc2 and Glc3, and then the model was refined with a Powell minimization procedure provided by X-PLOR

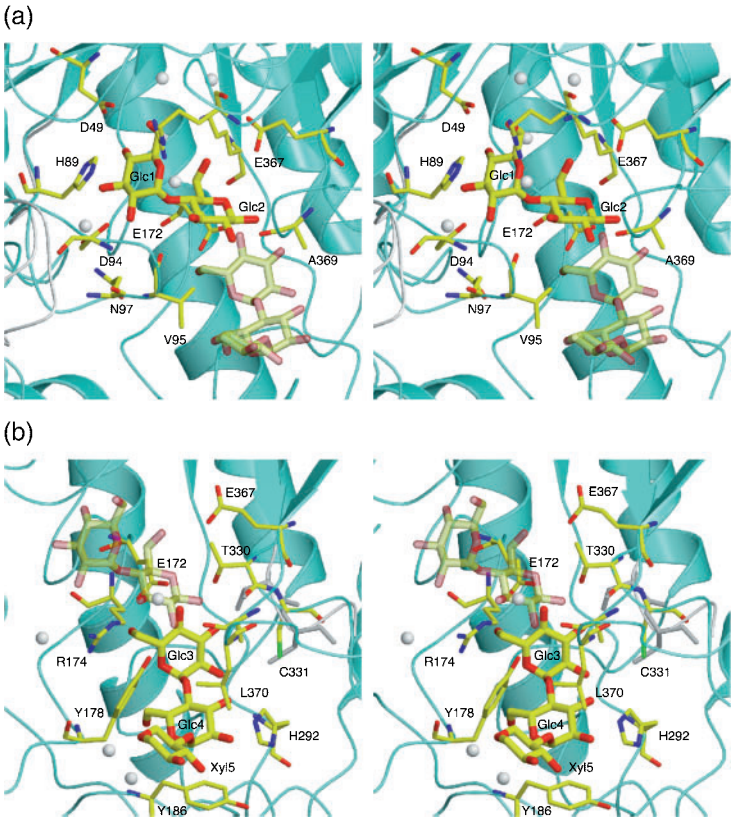

Fig. 5. **Close-up views of the enzyme-saccharide interaction of maltose (a) and GGX (b) in the active site cleft.** A maltose molecule is bound at subsites 1 and 2, and a GGX at subsites 3 to 5. Each saccharide residue was named according to the subsite number. For comparison of the binding sites, maltose and GGX are shown paler in (b) and (a), respectively. In (b), Thr-330 and Cys-331 in the structure of the free β-amylase are presented as white sticks to show the notable shifts toward the cleft on the binding of GGX.

allowing movement of Glc 2 and Glc 3 using only energy terms. The refined model produced by only slight rotations of Glc2 (*ca.* 10°) and Glc3 (*ca.* 20°) from the crystal structure led to a G5 model with good overall stereochemistry, but with an unfavorable dihedral angle of the α-1,4-glucosidic linkage between the two glucose residues implying high potential energy (*20*). In particular, the O2 atom of Glc2 is close to the C4 atom of the pyranose ring of Glc3, the distance being only 2.9 Å. If substrates are forced to adopt such an energetically unfavorable conformation by binding to the catalytic site, pyranose ring distortion of the glucose at subsite 2 might be caused, as observed in the crystal structure of maltotetraose-forming exo-α-amylase in a complex with maltotetraose, where the glucose residue of the saccharide at the cleavage site exhibites a half-chair conformation (*21*).

Substrate Recognition Revealed by the Binding Modes of GGX and Maltose—Based on the subsite structure of BCM β-amylase (Fig. 3b), it is expected that glucose and maltose should be also bound at subsites 3 and/or 4. We compared the five enzyme/inhibitor complexes and a free form of BCM β-amylase together with the previously reported β-amylase/maltose complexes (*4*, *6*, *7*). However, we could not find any structural evidence that could account for the absence of maltose and glucose at subsites 3 and 4 in the present structures. The soaking conditions for maltose and glucose in the crystals might be unsuitable for their binding at subsites 3 and 4. On the other hand, in the β-amylase/maltose complex and the β-amylase/GGX complex, which were prepared under similar conditions, the maltose and GGX were bound at different places in the active site. Nitta *et al*. have inferred from the results of an inhibition study that β-amylase binds GGX at subsites 1 to 3 in the active site (*12*). However, contrary to expectation, structural analysis revealed that GGX is bound at subsites 3 to 5. The binding mode of GGX indicates strongly that the β-amylase strictly recognizes the glucose residue at subsite 3, specifically the hydroxyl group at C-6 of glucopyranose, and that subsite 5 with lower affinity than those of subsites 1 and 4 (Fig. 3b) (*2*) contributes significantly to the substrate binding.

In the β-amylase/GGX complex, the C-6 hydroxyl group of the glucose residue at subsite 3, which exhibits a

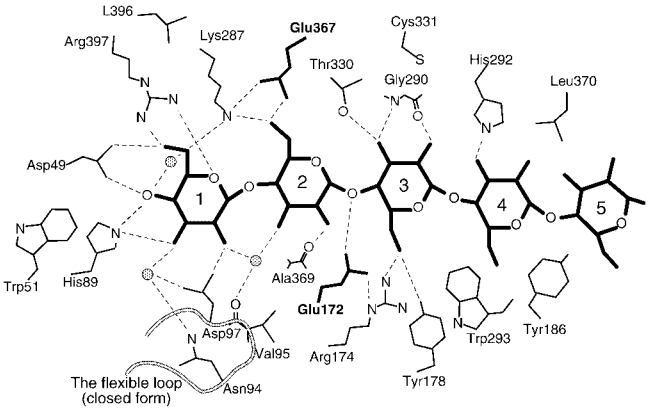

Fig. 6. **Schematic representation of the putative binding mode of a substrate, maltopentaose, based on the crystal structure.** Water molecules are presented as gray spheres. Possible hydrogen bonds are shown by dashed lines.

negative subsite affinity (Fig. 3b), forms hydrogen bonds with the side chain atoms of Glu-172 (OE2), Arg-174 (NE1), and Tyr-178 (OH), suggesting the importance of the hydroxyl group for the saccharide binding to the enzyme. The reducing end xylose of GGX lacks the CH_2OH group at the C-5 position of glucose. This lack of the hydroxyl group is supposed to prevent the binding of a xylose residue to subsite 3 because of insufficient contact with the enzyme, and hence the GGX cannot occupy subsites 1 to 3. The fact that only one molecule of maltose is bound to subsites 1 and 2 is consistent with the above consideration. Nitta *et. al*. have reported that other than GGX, *O*-α-D-xylopyranosyl-(1→4)-*O*-α-D-glucopyranosyl-(1→4)-D-glucopyranose (XGG), *O*-α-D-glucopyranosyl-(1→4)-*O*-α-D-xylopyranosyl-(1→4)-D-glucopyranose (GXG), and *O*-α-D-glucopyranosyl-(1→4)-*O*-α-D-xylopyranosyl-(1→4)-*O*-α-D-xylopyranosyl-(1→4)-D-glucopyranose (GXXG) are not hydrolyzed by soybean β-amylase, and do not inhibit the enzyme activity (*12*)**.** They have pointed out that a CH_2OH group at the C-5 position of the glucopyranose in a substrate plays a very important role in the catalytic action and the binding to the active site. Considering their results and the present X-ray crystallographic results together, it is suggested that (i) β-amylase recognizes a substrate in a maltose unit from the reducing end, and (ii) if at least one of the three glucose residues from the nonreducing end of a maltooligosaccharide is replaced by xylose, it cannot bind to the active site at subsites 1 to 4.

The maltose moiety of GGX could occupy subsites 3 and 4, but maltose did not bind there. Considering GGX is a derivative with a xylose moiety at the reducing end of maltose, additional binding affinity for the xylose residue may be responsible for the binding of GGX at subsites 3 to 5. The xylose residue at subsite 5 predominantly undergoes hydrophobic interactions with Leu-370 (Fig. 5b). If a glucose moiety instead of a xylose one is bound at subsite 5, the hydroxyl group at the C-6 position of the glucose moiety would not interact with the subsite. Therefore, the mode of binding of GGX is considered to correspond to a non-productive binding of maltotriose.

Irreversible Inactivation of the β-Amylase by Affinity-Labeling Reagents—Nitta *et al*. (*12*) proposed an irreversible inactivation mechanism for soybean β-amylase with α-EPG, as follows: Firstly, the protonated (acid) catalyst donates a proton to the epoxyl oxygen of the inhibitor. The activated epoxide undergoes nucleophilic attack by the carboxylate anion of the deprotonated (base) catalyst, by which its ring is opened. The reaction is completed by the covalent bond (esteric bond) formation between the inhibitor and the deprotonated catalyst. The contribution of the two catalytic residues to the inactivation was estimated from the pH-dependency of the inactivation velocity, which is remarkably similar to that of the catalytic activity (*11*). Based on this reaction scheme (termed "Scheme I"), Glu-186 of soybean β-amylase, which formed the covalent bond to α-EPG, was inferred to be the deprotonated catalyst. The present structure analysis showed that Glu-172 of BCM β-amylase, which corresponds to Glu-186 of soybean β-amylase, forms a covalent bond to both α-EPG and α-EBG. On the contrary, Mikami *et al*. (*6*) suggested opposite roles for the glutamic acid residues based on the results of their structure analysis of the soybean β-amylase/maltose complex: Glu-186 and Glu-380 (corresponding to Glu-367 of BCM β-amylase) would act as protonated and deprotonated catalysts, respectively. Considering the catalytic mechanism of β-amylase, i.e. that the α-anomeric configuration of the glucosidic linkage of a substrate is inverted to the β-anomeric one in the product (maltose), the latter proposal for the catalytic residues seems to be more probable.

Another inactivation mechanism different from Scheme I may be possible: the carboxyl group of Glu-172 donates a proton to the epoxyl oxygen of an affinity-labeling reagent and becomes a carboxylate anion. Next, the activated epoxide undergoes nucleophilic attack by the carboxylate anion, and its ring is opened and the reaction is completed through an esteric bond formation. Such unique inactivation mechanism has been previously proposed in the case of *endo*-1,4-xylanase from *Trichoderma ressei* (*22*). In the xylanase/epoxyalkyl xyloside complexes, two inhibitors (4,5-epoxypentyl β- D-xyloside, X-O-C5, and 4,5-epoxypropyl β- D-xyloside, X-O-C3) were covalently bound to the nucleophile (Glu-86), which supported a reaction scheme proposed for the xylanase (*23*) similar to Scheme I. On the other hand, 3,4-epoxybutyl β-D-xyloside (X-*O*-C_4) formed a covalent bond with the acid/base catalyst (Glu-177), suggesting that the glutamic acid residue has dual roles of proton-donation and nucleophilic attack in the inactivation reaction. In the β-amylase, Glu-367 of the possible deprotonated catalyst possesses a nucleophilic water at the tip of its side chain, which is observed in the complex with an affinity-labeling reagent (Fig. 4), and therefore it does not seem to interact directly with a substrate nor an affinity-labeling reagent during hydrolysis or the inactivation reaction. Glu-367 might play a role in controlling the relative distance and orientation between α-EPG and the deprotonated Glu-172, in a pH-dependent manner. To confirm this hypothetical mechanism, further study on the relevancy of Glu367 to the inactivation is currently underway, using site-directed mutants as to the catalytic residues.

This work was performed with the approval of the Photon Factory Program Advisory Committee (Proposal No. 98G064). The coordinates have been deposited in the RSCB Protein Data Bank under accession codes 1J0Y, 1J0Z, 1J10, 1J11, and 1J12 for the structures of the complexes with glucose, maltose, GGX, α-EPG, and α-EBG, respectively. We are grateful to Drs N. Watanabe, M. Suzuki, N. Sakabe, and N. Igarashi for the technical assistance at the Photon Factory.

REFERENCES

1. Henrissat, B. and Davis, G. (1997) Structural and sequence-based classification of glycoside hydrolases. *Curr. Opin. Struct. Biol.* **7**, 637–644
2. Janecek, S. and Sevcik, J. (1999) The evolution of starch-binding domain. *FEBS Lett.* **456**, 119–125
3. Nitta, Y., Shirakawa, M., and Takasaki, T. (1996) Kinetic study of active site structure of β-amylase from *Bacillus cereus* var. *mycoides*. *Biosci. Biotechnol. Biochem.* **60**, 823–827
4. Mikami, B., Adachi, M., Kage, T., Sarikaya, E., Nanmori, T., Shinke, R., and Utsumi, S. (1999) Structure of raw starch-digesting *Bacillus cereus* β-amylase complexed with maltose. *Biochemistry* **38**, 7050–7061

5. Oyama, T., Kusunoki, M., Kishimoto, Y., Takasaki, Y., and Nitta, Y. (1999) Crystal structure of β-amylase from *Bacillus cereus* var. *mycoides* at 2.2 Å resolution. *J. Biochem.* **125**, 1120–1130
6. Mikami, B., Degano, M., Hehre, E.J., and Sacchettini, J.C. (1994) Crystal structures of soybean β-amylase reacted with β-maltose and maltal: active site components and their apparent roles in catalysis. *Biochemistry* **33**, 7779–7787
7. Mikami, B., Yoon, H.J., and Yoshigi, N. (1999) The crystal structure of the sevenfold mutant of barley β-amylase with increased thermostability at 2.5 Å resolution. *J. Mol. Biol.* **285**, 1235–1243
8. Uitdehaag, J.C.M., Mosi, R., Kalk, K.H., van der Veen, B.A., Dijkhuizen, L., Withers, S.G., and Dijkstra, B.W. (1999) X-ray structures along the reaction pathway of cyclodextrin glycosyltransferase elucidate catalysis in the α-amylase family. *Nat. Struct. Biol.* **6**, 432–436
9. van der Veen, B.A., Uitdehaag, J.C., Penninga, D., van Alebeek, G.J., Smith, L.M., Dijkstra, B.W., and Dijkhuizen, L. (2000) Rational design of cyclodextrin glycosyltransferase from *Bacillus circulans* strain 251 to increase α-cyclodextrin production. *J. Mol. Biol.* **296**, 1027–1038
10. Sorimachi, K., Le Gal-Coëffet, M.F., Williamson, G., Archer, D.B., and Williamson, M.P. (1997) Solution structure of the granular starch binding domain of *Aspergillus niger* glucoamylase bound to β-cyclodextrin. *Structure* **5**, 647–651
11. Isoda, Y. and Nitta, Y. (1986) Affinity labeling of soybean β-amylase with 2,3-epoxypropyl α-D-glucopyranoside. *J. Biochem.* **99**, 1631–1637
12. Nitta, Y., Isoda, Y., Toda, H., and Sakiyama, F. (1989) Identification of glutamic acid 186 affinity-labeled by 2, 3-epoxypropyl α- D-glucopyranoside in soybean β-amylase. *J. Biochem.* **105**, 573–576
13. Nitta, Y., Suzuki, A., and Takeo, K. (1996) Actions of α- and β-amylases to tri- and tetra-saccharides containing xylose. *Oyo Toshitsu Kagaku (J. Appl. Glycosci.)* **43**, 167–172
14. Sakabe, N. (1991) X-ray diffraction data collection system for modern protein crystallography with a Weissenberg camera and an imaging plate using synchrotron radiation. *Nuclear Instr. Methods Physics Res.* **A303**, 448–463
15. Otwinowski, Z. and Minor, W. (1997) Processing of X-ray diffraction data collected in oscillation mode. *Methods Enzymol.* **276**, 307–326
16. Jones, T.A., Zhou, J.Y., Cowan, S.W., and Kjeldgaard, M. (1991) Improved methods for building protein models in electron density maps and the location of errors in these models. *Acta Crystallogr.* **A47**, 110–119
17. Brünger, A.T., Kuriyan, J., and Karplus, M. (1987) Crystallographic R factor refinement by molecular dynamics. *Science* **235**, 458–460
18. Engh, R.A. and Huber, R. (1991) Accurate bond and angle parameters for X-ray protein structure refinement. *Acta Crystallogr.* **A47**, 392–400
19. Laskowski, R.A., MacArthur, M.W., Moss, D.S., and Thornton, J.M. (1993) PROCHECK: a program to check the stereochemical quality of protein structures. *J. Appl. Crystallogr.* **26**, 283–291
20. Tran, V. and Buleon, A. (1989) Relaxed potential energy surfaces of maltose. *Biopolymers* **28**, 679–690
21. Yosihoka, Y., Hasegawa, K., Matsuura, Y., Katsube, Y., and Kubota, M. (1997) Crystal structures of a mutant maltotetraose-forming exo-amylase cocrystallized with maltopentaose. *J. Mol. Biol.* **271**, 619–628
22. Havukainen, R., Törröen, A., Laitinen, T., and Rouvinen, J. (1996) Covalent binding of three epoxyalkyl xylosides to the active site of *endo*-1, 4-xylanase II from *Trichoderma ressei*. *Biochemistry* **35**, 9617–9624
23. Høj, P.B., Rodriguez, E.B., Stick, R.V., and Stone, B.A. (1989) Active site-directed inhibition by optically pure epoxyalkyl cellobiosides reveals differences in active site geometry of two 1,3-1,4-β-D-glucan 4-glucanohydrolases. The importance of epoxide stereochemistry for enzyme inactivation. *J. Biol. Chem.* **266**, 11628–11631
24. Esnouf, R.M. (1997). An extensively modified version of MolScript which includes greatly enhanced colouring facilities. *J. Mol. Graph.* **15**, 132–134
25. Kraulis, P.J. (1991) MOLSCRIPT: a program to produce both detailed and schematic plots of protein structures. *J. Appl. Crystallogr.* **24**, 946–950
26. Merritt, E.A. and Murphy, M.E.P. (1994) Raster3D Version 2.0—A program for photorealistic molecular graphics. *Acta Crystallogr.* **D50**, 869–873